

Infrared and Raman spectroscopic study of $\text{Zn}_{1-x}\text{Mn}_x\text{Se}$ materials grown by molecular-beam epitaxy

T. R. Yang and C. C. Lu

Department of Physics, National Taiwan Normal University, Taipei 116, Taiwan, Republic of China

W. C. Chou

Department of Physics, Chung Yuan Christian University, Chungli, Taiwan, Republic of China

Z. C. Feng and S. J. Chua

Institute of Materials Research & Engineering, 3 Research Link, Singapore 117602

(Received 9 March 1999)

Molecular beam epitaxy and optical investigation of $\text{Zn}_{1-x}\text{Mn}_x\text{Se}$ epilayers over a large composition range ($x=0-0.78$), grown on GaAs (001) substrates, are reported. The far-infrared (FIR) reflectance and Raman scattering were performed to characterize the film quality and study their optical and electrical properties. FIR and Raman data provide experimental evidence on the intermediate-mode phonon behavior for $\text{Zn}_{1-x}\text{Mn}_x\text{Se}$ with x up to 0.78. Theoretical modeling fits of FIR spectra lead to the determination of optical parameters such as mode frequency, strength, damping constant, and electrical properties of dielectric constant, carrier concentration, mobility, conductivity, and effect mass, and their dependence on the Mn composition. Values of force constants of $F_{\text{MnSe}} = 17.1 \times 10^4 \text{ dyn cm}^{-1}$ and $F_{\text{ZnSe}} = 14.7 \times 10^4 \text{ dyn cm}^{-1}$, and the high-frequency limit dielectric constant of MnSe, $\epsilon_\infty = 5.4$, are obtained. [S0163-1829(99)07147-7]

I. INTRODUCTION

$\text{Zn}_{1-x}\text{Mn}_x\text{Se}$ is a wide band-gap ternary material, belonging to the II-Mn-VI group of semimagnetic or diluted magnetic semiconductors (DMS).¹ Because of their important semiconducting, optical, and magnetic properties for basic investigation and application prospects, DMS, including $\text{Zn}_{1-x}\text{Mn}_x\text{Se}$, and related structures have been the subject of extensive studies in the past two decades.¹⁻⁴ $\text{Zn}_{1-x}\text{Mn}_x\text{Se}$ has its energy gap tunable between 2.7–3.4 eV, depending on the Mn composition and the applied magnetic field.¹ Magnetic ions, Mn^{2+} , are random substituted with the Zn^{2+} in the cation positions, leading to interesting magneto-optical properties, such as a giant Zeeman splitting of the band edges.⁵ This has been utilized to obtain spin-dependent quantum confinement in tailored structures.^{6,7} $\text{ZnSe}/\text{Zn}_{1-x}\text{Mn}_x\text{Se}$ quantum well (QW) and superlattice (SL) structures are promising for next generation electro-optical and photonic devices.⁸⁻¹⁰

Bulk $\text{Zn}_{1-x}\text{Mn}_x\text{Se}$ has been prepared previously by the Bridgman method with a zinc-blende structure for $x < 0.35$ and a wurtzite structure for $0.35 < x < 0.57$.¹¹ Efforts have been made on the growth of epitaxial $\text{Zn}_{1-x}\text{Mn}_x\text{Se}$ films by various techniques, such as molecular beam epitaxy (MBE), metalorganic chemical vapor deposition (MOCVD), pulsed laser evaporation and epitaxy (PLEE), atomic layer epitaxy (ALE) and radio frequency sputtering.¹² Using the MBE technique, thick (1–3 μm) $\text{Zn}_{1-x}\text{Mn}_x\text{Se}$ epilayers with zinc-blende structure over the $0 \leq x \leq 0.66$ composition range,¹³ $\text{ZnSe}/\text{Zn}_{1-x}\text{Mn}_x\text{Se}$ QW and SL structures,⁶⁻¹⁰ and ZnSe/MnSe superlattices¹⁴ with both zinc-blende ZnSe and MnSe have also been successfully grown. Based on the fact that the atomic radius of Mn (1.79 Å) is larger than that of Zn (1.53

Å), it would be difficult to dope a large concentration of Mn atoms into the lattice of as-deposited $\text{Zn}_{1-x}\text{Mn}_x\text{Se}$ layers.¹² More epitaxial $\text{Zn}_{1-x}\text{Mn}_x\text{Se}$ films and microstructures reported in recent years (after 1990) were focused in the low Mn concentrations.^{5,6,7,9,10,12,15,16} Efforts in growing high Mn composition and high quality $\text{Zn}_{1-x}\text{Mn}_x\text{Se}$ materials and structures are needed for the further development of these promising materials and microstructures.

Infrared (IR) and Raman spectroscopy are sensitive, non-destructive and useful tools for the characterization of semiconductor materials and structures.^{17,18} They can provide information on lattice properties, crystalline perfection, impurities, defects, strain, phase transition and alloy compositions. It has been reported for the Raman scattering of high-pressure phase transition in bulk $\text{Zn}_{1-x}\text{Mn}_x\text{Se}$ ($0 \leq x \leq 0.30$),¹⁹ the resonant Raman scattering of longitudinal optical (LO) phonons in bulk cubic single crystal $\text{Zn}_{1-x}\text{Mn}_x\text{Se}$ ($x=0,0.03,0.1$) near the E_0 gap,²⁰ Raman spectra of RF sputtered $\text{Zn}_{1-x}\text{Mn}_x\text{Se}$ ($x=0.04,0.15,0.19,0.27,0.32$) thin films,¹² and a far-infrared reflection and transmission study on long-wavelength optical phonons in bulk $\text{Zn}_{1-x}\text{Mn}_x\text{Se}$ ($x=0.18,0.31$).²¹ The results demonstrated that $\text{Zn}_{1-x}\text{Mn}_x\text{Se}$ exhibits an intermediate mode behavior for the optical phonons, which is similar to the case of $\text{Zn}_{1-x}\text{Mn}_x\text{Te}$,²² and in contrast with $\text{Cd}_{1-x}\text{Mn}_x\text{Te}$,²² that exhibits a two-mode behavior for the optical phonons. But the experimental evidence was based upon a relatively small range of Mn compositions, $x \leq 0.33$ for bulk $\text{Zn}_{1-x}\text{Mn}_x\text{Se}$,¹⁹ and $x \leq 0.32$ for RF sputtered film $\text{Zn}_{1-x}\text{Mn}_x\text{Se}$.¹²

In this paper, we report on the growth and optical characterization of epitaxial $\text{Zn}_{1-x}\text{Mn}_x\text{Se}$ with Mn composition variation from 0% up to 78% by a molecular beam epitaxy

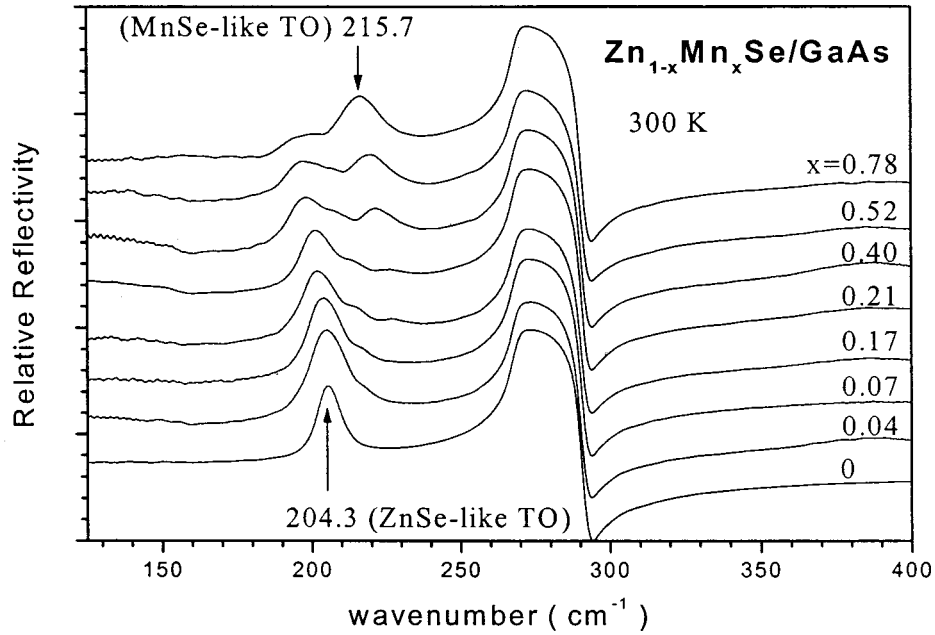


FIG. 1. The FIR reflectance spectra of $Zn_{1-x}Mn_xSe/GaAs$ for Mn compositions $x=0$ to 0.78 at 300 K.

technique. Far-infrared and Raman scattering spectra of eight MBE-grown $Zn_{1-x}Mn_xSe$ over a large range Mn composition of $0 \leq x \leq 0.78$ were investigated. The optical phonon behavior, conductivity, dielectric constant, and other optical parameters are analyzed by a dielectric response model. A series of optical and electrical parameters are deduced for $Zn_{1-x}Mn_xSe$ dependent on the Mn composition. Results are presented and discussed.

II. EXPERIMENT

$Zn_{1-x}Mn_xSe$ epilayers used in this study were grown on GaAs(001) substrates by an EPI 620 MBE system. High-energy electron diffraction (RHEED) was used to monitor the structure of the layers during growth. The Mn composition was determined by the energy dispersive x ray (EDX) for each sample. Energy gaps were measured from photoluminescence (PL) and photoreflectance (PR) experiments.²³

The IR reflectance spectra at near normal incidence in far-infrared range, $60\text{--}700\text{ cm}^{-1}$, were measured by way of a Bruker IFS 120 HR Fourier transform infrared (FTIR) spectrometer with resolution better than 1 cm^{-1} , and in the temperature range of $80\text{--}300\text{ K}$. Raman measurements were performed in the back-scattering geometry between $10\text{--}300\text{ K}$ by using a Dilor X-Y 800 modular laser Raman spectrometer with CCD photon-counting electronics. Raman spectra were excited by the Ar^+ laser 514.5-nm line and with laser power less than 25 mW to avoid the heating effect.

III. EXPERIMENTAL RESULTS

A. Infrared reflectance

Figure 1 shows the FTIR reflection spectra of eight $Zn_{1-x}Mn_xSe/GaAs$ with $x=0$ to 0.78, measured at 300 K, while Fig. 2 exhibits the FTIR spectra of a typical $Zn_{0.48}Mn_{0.52}Se/GaAs$ at a temperature of $80\text{--}300\text{ K}$. For mixed crystal, there are two x -dependent transverse modes, denoted TO_1 and TO_2 , with oscillator strengths S_1 and S_2 ,

and frequencies ω_{T1} and ω_{T2} , respectively. To these transverse modes, there are associated longitudinal modes denoted LO_1 and LO_2 with frequencies ω_{L1} and ω_{L2} , respectively.^{17,24} The vibration mode occurring in 204 cm^{-1} for $x=0$ at 300 K is referred to as the ZnSe-like mode (TO_2). We can also assign the MnSe-like mode (TO_1) to 215 cm^{-1} for $x=0.78$. We observed that the ZnSe-like TO mode is around $195\text{--}205\text{ cm}^{-1}$ for different Mn concentration samples at 300 K, while the MnSe-like TO vibration mode is clearly around $215\text{--}225\text{ cm}^{-1}$ for $x > 0.17$. There is a small mode appearing in 215 cm^{-1} for $x=0.07$ that is not clear at $x=0.04$. Obviously, all the resonance frequencies show temperature dependence. The vibration frequencies have $3\text{--}4\text{ cm}^{-1}$ blueshift for the ZnSe-like TO mode and $\sim 5\text{ cm}^{-1}$ blueshift for the MnSe-like TO mode when temperature is controlled from room temperature down to liquid nitrogen temperature, as seen from Fig. 2.

B. Raman scattering

Figure 3 shows Raman spectra from five of these DMS at 300 K for $x=0$ to 0.78. The Raman peak at 291 cm^{-1} is

TABLE I. The TO phonon mode parameters derived by dielectric function fitting.

x	S	ZnSe-like mode		MnSe-like mode		
		$\omega_{TO}(\text{cm}^{-1})$	$\gamma(\text{cm}^{-1})$	S	$\omega_{TO}(\text{cm}^{-1})$	$\gamma(\text{cm}^{-1})$
0	1.48	204.3	3.07			
0.04	1.99	203.4	3.52			
0.07	1.48	203.3	3.64			
0.17	1.79	200.7	6.44	0.08	225.0	8.26
0.21	1.79	200.7	6.72	0.08	223.9	8.26
0.4	1.37	197.8	7.93	0.36	219.7	5.92
0.52	1.13	196.5	9.64	0.46	218.0	5.65
0.78	0.81	195.7	11.03	0.95	215.7	4.76

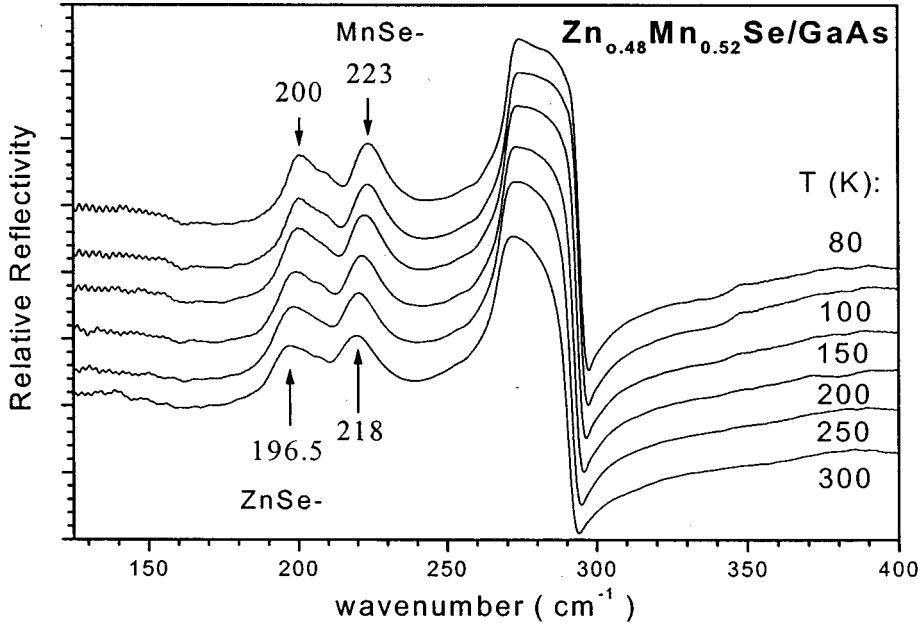


FIG. 2. The $\text{Zn}_{0.48}\text{Mn}_{0.52}\text{Se}/\text{GaAs}$ FIR spectrum for different temperature. The ZnSe-like and MnSe-like TO phonon mode have 3–4 cm^{-1} blueshift when temperature decreases from 300 K down to 80 K.

identified as the longitudinal optical (LO) phonon from the GaAs substrate. The Raman shift of ZnSe LO vibration mode occurs at 252 cm^{-1} , which can be assigned as the LO_1 mode at $x=0$. With increasing x value from $x=0$ to 0.52, the LO_1 vibration mode has a 3-cm^{-1} blueshift, and the mode intensity weakens. For $x=0.78$, the LO_1 mode is too weak to be recognized. The LO_1 mode also shows the temperature dependence that all $\text{Zn}_{1-x}\text{Mn}_x\text{Se}$ epilayers with different Mn concentrations have a blueshift of $3\text{-}4\text{-cm}^{-1}$ when temperature varies from 300 K down to 10 K. This can be seen from Fig. 4 on a $\text{Zn}_{1-x}\text{Mn}_x\text{Se}/\text{GaAs}$ with $x=0.21$.

IV. ANALYSIS AND DISCUSSION

A. Theoretical fits of FIR reflectance

From a classical model, the FIR dielectric response function can be expressed as^{17,24}

$$\varepsilon(\omega) = \varepsilon_{\infty} + \frac{S_j \omega_{Tj}^2}{(\omega_{Tj}^2 - \omega^2 - i\gamma_j \omega)} - \frac{\omega_p^2}{\omega \left(\frac{\omega + i}{\tau} \right)}, \quad (1)$$

where ε_{∞} is the high frequency dielectric constant, ω_{Tj} , S_j , and γ_j are the frequency, strength, and damping constant of the j th TO mode, respectively. The last term in the equation represents the free carrier contribution with a carrier scattering time τ and a plasma frequency

$$\omega_p = \left(\frac{4\pi n e^2}{m^*} \right)^{1/2}, \quad (2)$$

where n is the carrier concentration and m^* is the effective mass. Computer fittings were performed for all the FIR spectra in Fig. 1. The frequencies and other parameters of the optical modes at 300 K obtained from these theoretical fits

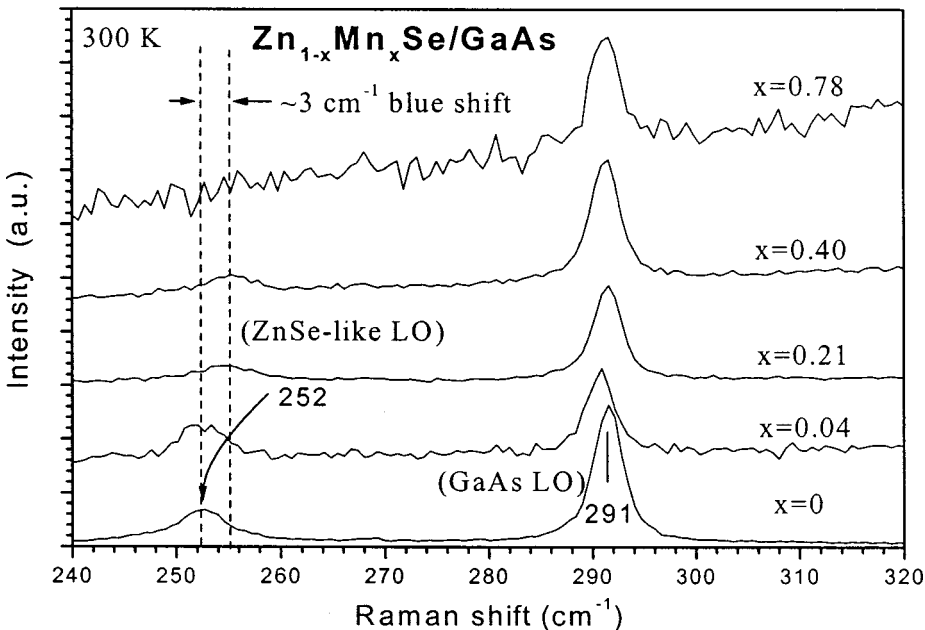


FIG. 3. Raman scattering spectra of $\text{Zn}_{1-x}\text{Mn}_x\text{Se}$ for different x values at 300 K. LO_1 phonon mode was revealed at 258 cm^{-1} for ZnSe thin film, and has 3 cm^{-1} blueshift when Mn concentration increased to 0.52.

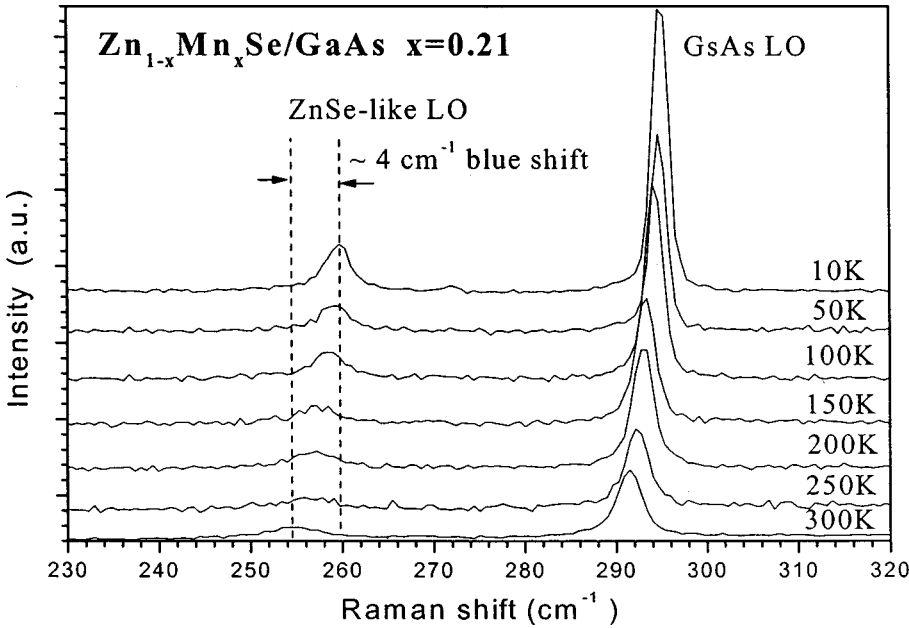


FIG. 4. Temperature dependent Raman spectra of a $\text{Zn}_{1-x}\text{Mn}_x\text{Se}/\text{GaAs}$ with $x=21\%$ from 10 to 300 K.

are collected in Table I. With increasing Mn concentration from $x=0$ to 0.78, the ZnSe-like TO mode has a 9-cm^{-1} red shift. MnSe-like TO mode has a 10-cm^{-1} red shift from $x=0.17$ to 0.78. The ZnSe-like TO, MnSe-like TO and LO_1 vibration modes versus x values are shown in Fig. 5. The values of mode frequency, strength, and phonon relaxation factor or damping constant γ of each band depend on the detailed composition of samples. The Mn concentration dependence of the strength of ZnSe-like and MnSe-like TO phonon modes is illustrated in Fig. 6. This shows that the strength of ZnSe-like mode is decreasing and the strength of MnSe-like mode is increasing with increasing Mn composition.

B. Discussion on phonon mode parameters

From the dielectric function ϵ for a system with two oscillators, the strength of TO_1 and TO_2 can be expressed as²⁴

$$S_1 \omega_{T1}^2 = \epsilon_\infty \frac{(\omega_{L1}^2 - \omega_{T1}^2)(\omega_{L2}^2 - \omega_{T1}^2)}{\omega_{T2}^2 - \omega_{T1}^2}, \quad (3)$$

$$S_2 \omega_{T2}^2 = \epsilon_\infty \frac{(\omega_{L1}^2 - \omega_{T2}^2)(\omega_{L2}^2 - \omega_{T2}^2)}{\omega_{T1}^2 - \omega_{T2}^2}. \quad (4)$$

From Fig. 5, $\omega_{T1}^2 - \omega_{T2}^2$ varies between two ending values, i.e., about 1800 to 2700 ($1/\text{cm}^2$), and $\omega_{L1}^2 - \omega_{T1}^2$ and $\omega_{L1}^2 - \omega_{T2}^2$ are far away from zero. From Fig. 6, it is seen that as x approaches zero, S_1 approaches zero. Therefore, $\omega_{T1}^2 - \omega_{L2}^2$ should approach zero when x is close to zero from Eq. (3). On the contrary, $\omega_{L2}^2 - \omega_{T2}^2$ cannot vanish from Eq. (4) because S_2 is not small, as shown in Fig. 6. As x is larger, say $x=0.78$, the situation is reversed. Therefore, we can predict that the associated LO_2 mode frequency will approach

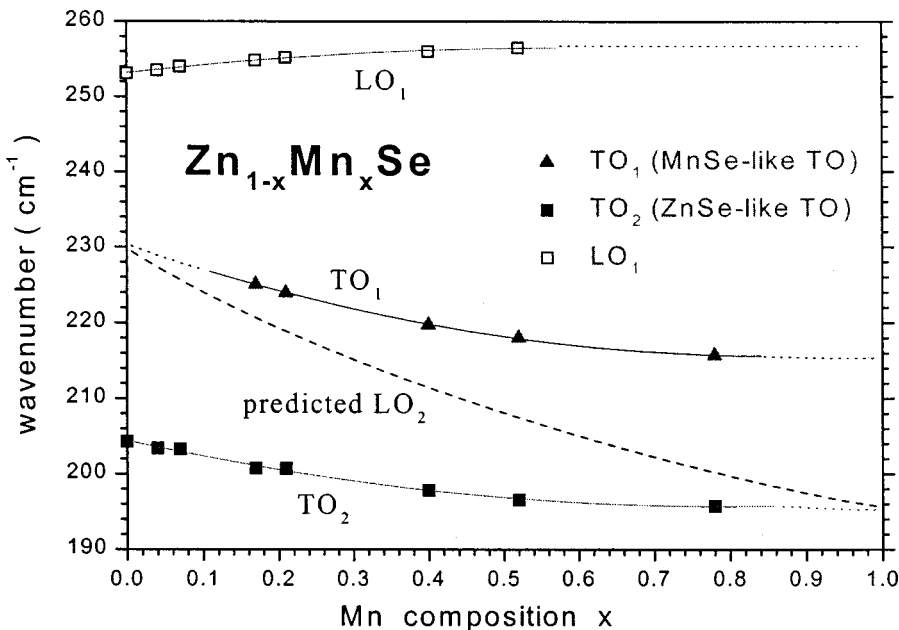


FIG. 5. Relationships of optical mode frequency versus x from epitaxial $\text{Zn}_{1-x}\text{Mn}_x\text{Se}$. The dotted line is the guide to the eye, and the dash line is the predicted LO_2 . This plot shows the $\text{Zn}_{1-x}\text{Mn}_x\text{Se}$ mixed crystal has an intermediate-mode behavior for optical phonons.

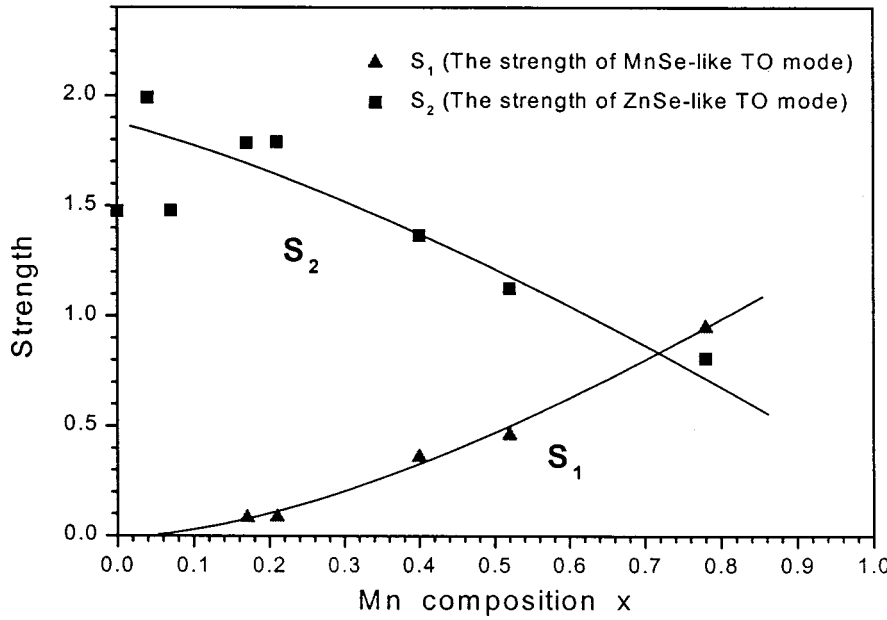


FIG. 6. The relationship of the mode strength of TO_1 and TO_2 versus the Mn composition x .

the frequency of TO_1 at $x \sim 0$ and will approach to the TO_2 frequency as $x \sim 1$. The predicted LO_2 mode is shown in Fig. 5 with the dashed line.

The mode behavior of $Zn_{1-x}Mn_xSe$ thin film shown in Fig. 5 is a typical intermediate-mode behavior. It shows that the Mn impurity mode in ZnSe lies between the LO and TO frequencies of ZnSe, displaying as a gap mode, while the Zn impurity mode in the MnSe lattice lies below the LO-TO range for MnSe-like phonons, as a local mode. It also shows that with increasing the x (Mn), the ZnSe:Mn gap mode splits into two branches of TO_1 and LO_2 . The LO_2 and TO_2 modes, when x (Mn) approaches 1, emerge into the ZnSe:Mn local mode.^{12,19,22,24} As a complementary work for previous results on bulk and film $Zn_{1-x}Mn_xSe$ with $x < 0.33$,^{12,19} our new FIR and Raman data from MBE-grown $Zn_{1-x}Mn_xSe$ provide the further experimental evidence on the intermediate-mode behavior of optical phonons for this dilute magnetic semiconductor material system with x up to 0.78.

C. Force constants

Force constant between anion and cation can be deduced from the impurity mode frequency. The impurity frequency at $x=0$ is about 230 cm^{-1} from the extended dotted line in Fig. 5. There exists the following relationship:²⁴

$$\sqrt{\frac{F_{MnSe}}{m_{Mn}}} = 230 \text{ cm}^{-1}, \quad (5)$$

where m_{Mn} is the mass of an Mn atom. Thus, the force constant $E_{MnSe} = 17.1 \times 10^4 \text{ dyn cm}^{-1}$ between Mn and Se atoms is obtained.

At another end of $x=1$, the impurity frequency is about 195 cm^{-1} . There is also a similar relationship:²⁴

$$\sqrt{\frac{F_{ZnSe}}{m_{Zn}}} = 195 \text{ cm}^{-1}, \quad (6)$$

where m_{Zn} is the mass of a Zn atom. Another force constant $F_{ZnSe} = 14.7 \times 10^4 \text{ dyn cm}^{-1}$ between Zn and Se atoms can also be obtained.

D. Electrical conductivity

Some electrical properties of $Zn_{1-x}Mn_xSe$ thin films can also be characterized by fitting the dielectric function. The obtained parameter data for the high-frequency limit dielectric constant, free carrier concentration, mobility, conductivity and effective mass are listed in Table II. With the weighted summation of the Clausius-Mossotti expressions for dielectric constant $\epsilon_\infty(\text{MnSe})$ of pure MnSe crystal and $\epsilon_\infty(\text{ZnSe})$ of ZnSe, we have²⁵

$$\frac{\epsilon_\infty(x) - 1}{\epsilon_\infty(x) + 2} = (1-x) \nu_{ZnSe} \frac{\epsilon_\infty(\text{ZnSe}) - 1}{\epsilon_\infty(\text{ZnSe}) + 2} + x \nu_{MnSe} \frac{\epsilon_\infty(\text{MnSe}) - 1}{\epsilon_\infty(\text{MnSe}) + 2}. \quad (7)$$

In Eq. (7), $\epsilon_\infty(x)$ is the high-frequency limit of the dielectric constant of the $Zn_{1-x}Mn_xSe$ epilayer, and ν_{ZnSe} and ν_{MnSe} denote the ratio between unit cell volume of pure ZnSe,

TABLE II. Electric properties of $Zn_{1-x}Mn_xSe$ characterized by dielectric function fitting.

x	ϵ_∞	Free carrier concentration (10^{18} cm^{-3})	Mobility ($\text{cm}^2/\text{V S}$)	Conductivity ($\Omega^{-1} \text{ cm}^{-1}$)	m^*/m_e
0	6.06	0.998	4447	710.1	0.53
0.04	6.02	1.015	2216	359.9	0.53
0.07	5.97	0.895	1416	202.7	0.53
0.17	5.94	0.729	744	86.8	0.51
0.21	5.92	1.096	355	62.2	0.52
0.4	5.82	1.038	263	43.7	0.51
0.52	5.83	1.290	292	60.2	0.49
0.78	5.61	0.672	153	16.5	0.49

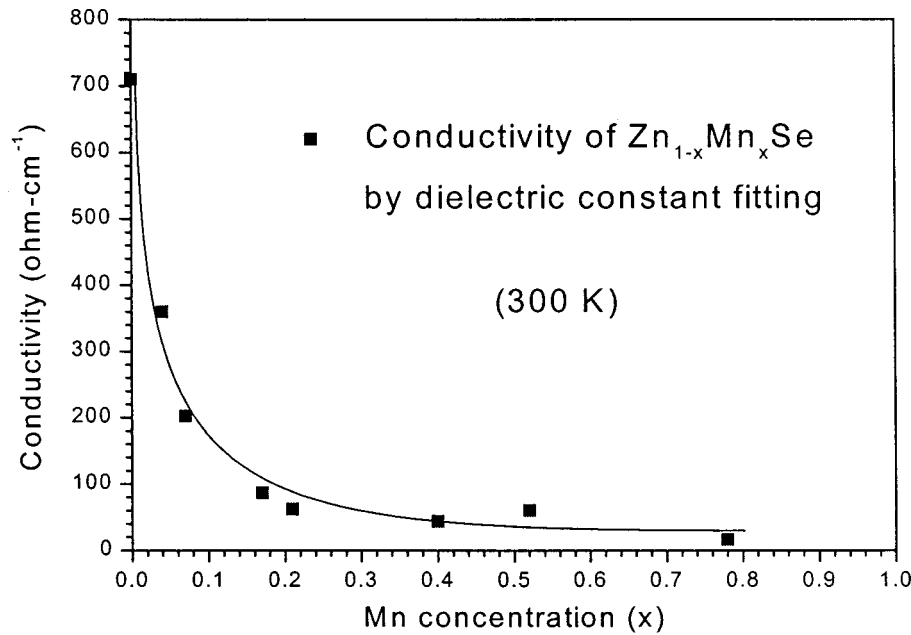


FIG. 7. The dependence of the conductivity of the $Zn_{1-x}Mn_xSe$ epilayer with the Mn composition x .

MnSe, and x -dependent unit cell volume of $Zn_{1-x}Mn_xSe$ material. We take both ν_{ZnSe} and ν_{MnSe} approaching 1 in our calculation. By using our experimental values of dielectric constant for $Zn_{1-x}Mn_xSe$, listed in Table II, we can obtain $\epsilon_{\infty}(MnSe)=5.4$.

We can also employ the linear approximation relation,²⁶

$$\epsilon_{\infty}(x) = x\epsilon_{\infty}(MnSe) + (1-x)\epsilon_{\infty}(ZnSe) \quad (8)$$

to obtain the value of $\epsilon_{\infty}(MnSe)$. Both ways lead to the same result. Our value is much higher than the previous reported result,²² and it is more reliable.

The values of conductivity versus x are illustrated in Fig. 7. It shows that the conductivity will drop down dramatically when Mn composition is increasing from 0 to $\sim 15\%$. For $x > 0.17$, the conductivity will slowly and almost linearly goes down with increasing the Mn composition. The effect mass of free carriers also drops linearly with the varied Mn concentration from the fitting results, listed in Table II.

V. CONCLUSIONS

In conclusion, we have grown a series of $Zn_{1-x}Mn_xSe$ epilayers, with a large range of Mn composition from 0 up to 78%, on GaAs(001) substrates by MBE technology. The far-infrared reflection spectra and Raman scattering show the good optical quality of these samples. FIR and Raman data

show the interesting intermediate-mode phonon behavior for this dilute magnetic semiconductor material system. Theoretical fits through a classical model with the FIR dielectric response function were performed on FIR reflectivity spectra of all the samples. Composition dependent optical parameters of transverse phonon mode frequency, strength, damping constant have been deduced. With an increase of Mn composition x , the ZnSe-like TO phonon mode frequency and strength decrease, damping factor increases, while the MnSe-like TO phonon mode frequency and strength increase, and damping factor decreases with increasing x . Detailed analyses of FIR reflectance and dielectric function have also led to the knowledge of electrical properties of $Zn_{1-x}Mn_xSe$ ($0 \leq x \leq 0.78$), including the high-frequency limit dielectric constant, free carrier concentration, mobility, conductivity and effective mass. With increasing x , ϵ_{∞} and m^* decrease slightly, while mobility and conductivity decrease greatly. This predicts a strong effect of Mn composition on the film electrical properties of mobility and conductivity, which is useful for device application of this DMS material. The force constants of two ending binary materials are obtained with $F_{MnSe} = 17.1 \times 10^4 \text{ dyne cm}^{-1}$ and $F_{ZnSe} = 14.7 \times 10^4 \text{ dyne cm}^{-1}$. A value of the high-frequency limit dielectric constant of MnSe, $\epsilon_{\infty} = 5.4$, is obtained by way of Clausius-Mossotti law and linear approximation.

¹J. K. Furdyna, J. Appl. Phys. **64**, R29 (1988).

²*Diluted Magnetic Semiconductors, Semiconductors and Semimetals*, edited by J. K. Furdyna and J. Kossut (Academic Press, Boston, 1988), Vol. 25.

³*Diluted Magnetic Semiconductors*, edited by Mukesh Jain (World Scientific, Singapore, 1991).

⁴*Widegap II-VI Compounds for Opto-electronic Applications*, edited by H. E. Ruda (Chapman & Hall, London, 1992).

⁵H. Abad, B. T. Jonker, W. Y. Yu, S. Stoltz, and A. Petrou, Appl.

Phys. Lett. **66**, 2412 (1995).

⁶W. C. Chou, A. Petrou, J. Warnock, and B. T. Jonker, Phys. Rev. Lett. **67**, 3820 (1991).

⁷N. Dai, H. Luo, F. C. Zhang, N. Samarth, M. Dobrowolska, and J. K. Furdyna, Phys. Rev. Lett. **67**, 3824 (1991).

⁸R. B. Bylisma, J. Kossut, W. M. Becker, L. A. Kolodziejski, R. L. Gunshor, and R. Frohne, J. Appl. Phys. **61**, 3011 (1987).

⁹U. Streller, N. Hoffmann, A. Shulzgen, J. Griesche, H. Babucke, F. Henneberger, and K. Jacobs, Semicond. Sci. Technol. **10**, 201

- (1995).
- ¹⁰T. Lebihen, A. Filoramo, E. Deleporte, J. Martinez-Pastor, Ph. Roussignol, C. Delalande, M. Zigone, and G. Martinez, *Phys. Rev. B* **55**, 9915 (1997).
- ¹¹R. B. Bylisma, W. M. Becher, J. Kossut, U. Debska, and D. Yoder-Short, *Phys. Rev. B* **33**, 8207 (1986).
- ¹²C. T. Tsai, D. S. Chuu, J. Y. Leou, and W. C. Chou, *Jpn. J. Appl. Phys., Part 1* **36**, 4427 (1997), and references therein.
- ¹³Y. Hefetz, J. Nakahara, A. V. Nurmikko, L. A. Kolodziejski, R. L. Gunshor, and S. Datta, *Appl. Phys. Lett.* **47**, 989 (1985).
- ¹⁴M. Kobayashi, R. L. Gunshor, and L. A. Kolodziejski, in *Wide-gap II-VI Compounds for Opto-electronic Applications* (Ref. 4), pp. 124–164.
- ¹⁵W. C. Chou, A. Twardowski, K. Chern-Yu, F. R. Chen, C. R. Hua, B. T. Jonker, W. Y. Yu, S. T. Lee, and A. Petrou, *J. Appl. Phys.* **75**, 2936 (1994).
- ¹⁶C. D. Poweleit, L. M. Smith, and B. T. Jonker, *Phys. Rev. B* **55**, 5062 (1997).
- ¹⁷S. Perkowitz, *Optical Characterization of Semiconductors: Infrared, Raman, and Photoluminescence Spectroscopy* (Academic Press, London, 1993).
- ¹⁸*Optical Characterization of Epitaxial Semiconductor Layers*, edited by G. Bauer and W. Richter (Springer-Verlag, Berlin, 1996).
- ¹⁹A. K. Arora, E.-K. Suh, U. Debska, and A. K. Ramdas, *Phys. Rev. B* **37**, 2927 (1988).
- ²⁰W. Limmer, H. Leiderer, K. Jakob, W. Gebhardt, W. Kauschke, A. Cantarero, and C. Trallero-Giner, *Phys. Rev. B* **42**, 11 325 (1990).
- ²¹W. Lu, P. L. Liu, G. L. Shi, S. C. Shen, and W. Giriat, *Phys. Rev. B* **39**, 1207 (1989).
- ²²D. L. Peterson, A. Petrou, W. Giriat, A. K. Ramdas, and S. Rodriguez, *Phys. Rev. B* **33**, 1160 (1986).
- ²³W. C. Chow, C. S. Ro, D. Y. Hong, C. S. Yang, C. Y. Lin, T. Y. Lin, K. C. Chiu, T. R. Yang, C. M. Lin, D. S. Chuu, and W. Y. Uen, *Chin. J. Phys.* **36**, 120 (1998).
- ²⁴L. Genzel, T. P. Martin, and C. H. Perry, *Phys. Status Solidi B* **62**, 83 (1974).
- ²⁵I. F. Chang and S. S. Mitra, *Adv. Phys.* **20**, 359 (1971).
- ²⁶I. F. Chang and S. S. Mitra, *Phys. Rev.* **172**, 924 (1968).